NANO · MICRO small
www.small-journal.com

Observation of Exchange Interaction in Iron(II) Spin Crossover Molecules in Contact with Passivated Ferromagnetic Surface of Co/Au(111)

Hongyan Chen, Hung-Hsiang Yang, Timo Frauhammer, Haoran You, Qing Sun, Peter Nagel, Stefan Schuppler, Ana Belén Gaspar, José Antonio Real, and Wulf Wulfhekel*

Dedicate to this Work to the Late Eric Beaurepaire, who was the Inspiration for this Project

Spin crossover (SCO) complexes sensitively react on changes of the environment by a change in the spin of the central metallic ion making them ideal candidates for molecular spintronics. In particular, the composite of SCO complexes and ferromagnetic (FM) surfaces would allow spin-state switching of the molecules in combination with the magnetic exchange interaction to the magnetic substrate. Unfortunately, when depositing SCO complexes on ferromagnetic surfaces, spin-state switching is blocked by the relatively strong interaction between the adsorbed molecules and the surface. Here, the Fe(II) SCO complex $[Fe^{II}(Pyrz)_2]$ (Pyrz = 3,5-dimethylpyrazolylborate) with submonolayer thickness in contact with a passivated FM film of Co on Au(111) is studied. In this case, the molecules preserve thermal spin crossover and at the same time the high-spin species show a sizable exchange interaction of > 0.9 T with the FM Co substrate. These observations provide a feasible design strategy in fabricating SCO-FM hybrid devices.

1. Introduction

The spin crossover (SCO) phenomenon has emerged as one of the most appealing platforms for investigating the switching of molecular electronic states and assessing their integration as an active function in novel electronic and spintronic devices. Among SCO compounds, those based on the Fe(II) ion are the most investigated since they offer the richest chemical and phenomenological versatility. They switch between the high-spin ($t_{2g}^4 e_g^2$, HS) and low-spin ($t_{2g}^6 e_g^0$, LS) electronic states in a reversible and detectable fashion in response to external stimuli (temperature, pressure, light irradiation, soft X-rays and inclusion of guest molecules). Furthermore, the intrinsic population/depopulation of the antibonding e_g orbitals is at the origin of the changes in shape and size of the Fe(II) centers (average Fe-N bond length ca. 0.2 Å larger in the HS state). These structural changes may spread cooperatively across the bulk material conferring strong cooperative ON-OFF hysteretic behavior to the magnetic, optical, dielectric and structural properties, which may be exploited for practical applications.[1–6] An imperative condition to realize SCO-based practical applications requires to demonstrate that the spin-state switching behavior can be operative at nanometric scale, for example, nanoparticles, ultrathin films, and even single molecules.[7–17]

H. Chen, H.-H. Yang, T. Frauhammer, H. You, W. Wulfhekel
Physikalisches Institut
Karlsruhe Institute of Technology (KIT)
76131 Karlsruhe, Germany
E-mail: hongyan.chen@kit.edu

Q. Sun
Laboratory for Electron Microscopy
Karlsruhe Institute of Technology (KIT)
76131 Karlsruhe, Germany

The ORCID identification number(s) for the author(s) of this article can be found under https://doi.org/10.1002/smll.202300251.

DOI: 10.1002/smll.202300251

P. Nagel, S. Schuppler
Electron Spectroscopy Group
Institute for Quantum Materials and Technologies (IQMT)
Karlsruhe Institute of Technology (KIT)
76021 Karlsruhe, Germany

P. Nagel, S. Schuppler
Karlsruhe Nano Micro Facility (KNMFi)
Karlsruhe Institute of Technology (KIT)
76344 Eggenstein-Leopoldshafen, Germany

A. B. Gaspar, J. A. Real
Institut de Ciència Molecular (ICMol)
Universitat de València
C/Catedrático José Beltrán Martínez 2, 46980 Paterna, Valencia, Spain

W. Wulfhekel
Quantum Control Group
Institute for Quantum Materials and Technologies (IQMT)
Karlsruhe Institute of Technology (KIT)
76021 Karlsruhe, Germany

Obviously, given the cooperative nature of the SCO phenomenon the transition from the bulk compound to the nanometer-size may have important costs in terms of fundamental parameters of the SCO (i.e., completeness, hysteresis width and characteristic temperatures). For example, the deposition of SCO molecules as thick films on silicon substrates lead to the loss of hysteretic behavior during thermal SCO transition even though the silicon substrates are relatively inert.[18] Further depositing SCO molecules onto metal substrates often results in the loss of the switchability and/or leads to decomposition of the molecules due to the strong chemical interaction between molecules and surface.[19,20] Therefore, to maintain SCO, either intrinsically inert and robust molecules and/or weakly interacting surfaces have been selected.[19,21–24] Indeed, the demonstrated ability to reversibly switch the spin state between LS and HS states at nanometric scale, for example, by external stimuli such as light,[25,26] X-ray,[27] voltage,[28] and temperature,[29] makes Fe(II) SCO complexes ideal candidates for molecular spintronics and promising application as building blocks for classical bits, sensors, and actuator devices.[9,19,30,31] Extensive research has focused on the SCO phenomenon regarding the practical properties of the SCO molecules itself, and combine systems like spin valves, heterostructures, etc.[32–34]

Thanks to the advances in design and synthesis of SCO complexes over decades, robust and vacuum sublimable SCO molecules are at hand. [Fe(bpz)$_2$phen] (bpz = dihydrobispyrazolylborate, phen = 1,10-phenanthroline) molecules in direct contact with highly oriented pyrolytic graphite keep their highly efficient thermal- and light-induced spin-state switching behavior.[35] In addition to the molecule design, by introducing a thin CuN insulating space layer in between the molecules and the Cu substrate, Fe(phen)$_2$(NCS)$_2$ molecules can show robust SCO and memristance.[19] More recently, it has been introduced a novel technique to combine SCO molecules with 2D materials building heterostructures in which the molecular spin switching induced volume change can in turn work as a strain effect to the 2D materials alter their electrical and optical properties.[32] It has been shown that [Fe^{II}(Pyrz)$_2$] maintains a bistable spin-state switching even when deposited directly onto metallic substrate like Au(111), Ag(111) and Cu(111).[21–23,26] All this progress pave the way for the control of the SCO properties at molecular scale and offer new routes to engineer the new materials combined with SCO molecules. Nevertheless, reports of the SCO molecules on magnetic surfaces are still scarce, and to the best of our knowledge, no work has reported successful combination of sub-monolayer (sub-ML) SCO molecules on magnetic substrate while maintaining the switching ability.

In this work, we report on experimental realization of the above-mentioned concept of SCO complexes on ferromagnetic (FM) substrates. We deposited sub-ML of [Fe^{II}(Pyrz)$_2$] molecules on Au passivated FM Co films on Au(111). The passivation not only serves to keep the SCO molecules and their switching intact but also allows an indirect exchange interaction across the Au layer.[36] The results demonstrated that the [Fe^{II}(Pyrz)$_2$] molecules in the HS state interact ferromagnetically with the FM Co film and maintain their SCO ability.

2. Results and Discussion

The molecular structure of [Fe^{II}(Pyrz)$_2$] is shown in **Figure 1**a.[37] The divalent iron ion Fe(II) is surrounded by six nitrogen atoms in octahedral symmetry thus the 3*d* orbitals split into e_g and t_{2g} levels. Bulk [Fe^{II}(Pyrz)$_2$] exhibits thermal SCO accompanied by an asymmetric thermal hysteresis showing equilibrium temperatures $T_{1/2}$, at which the HS and LS molar fraction are 0.5,

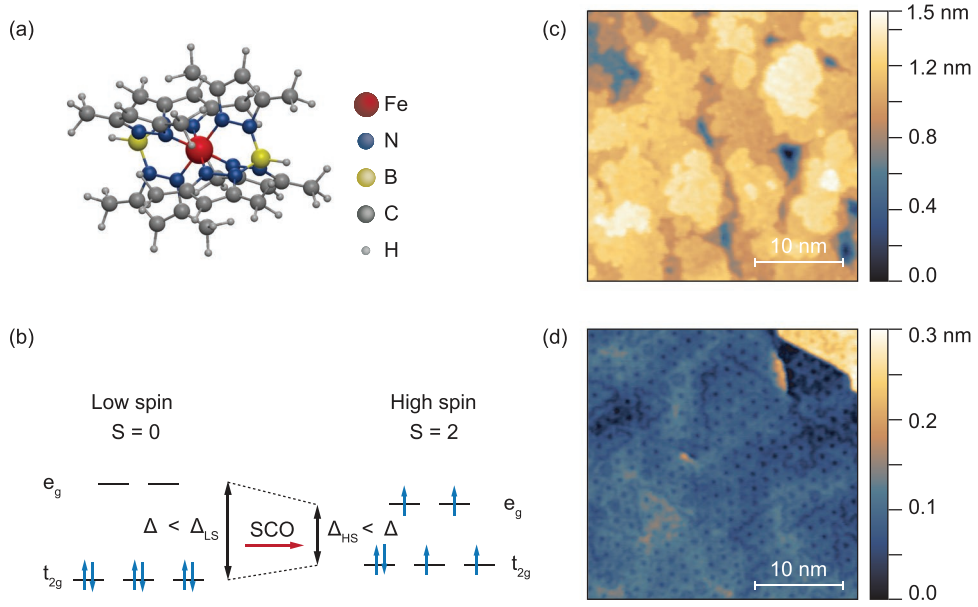

Figure 1. a) Schematic of a [Fe^{II}(Pyrz)$_2$] molecule. The central Fe(II) ion is surrounded by six nitrogen atoms in octahedral symmetry. b) Simplified electronic configurations of the Fe(II) SCO molecule. The interplay between the ligand field strength (Δ_{LS} or Δ_{HS}) and the spin pairing energy (Δ) determine the spin states. c,d) STM topography of Co film on Au(111) substrate before (c) and after (d) annealing process. The moiré pattern after annealing is indicative for a passivation by the Au overlayer. (U = 1 V, I = 300 pA).

of 174 and 199 K for cooling and heating, respectively.[37,38] The process is accompanied by a change in the Fe-N bond length, that is, a structural phase transition resulting in a change of the ligand fields. The corresponding electronic configurations of Fe(II) center in the two spin states are shown in Figure 1b. Depending on the strength of the ligand field ($\Delta_{LS,\ HS}$), the electrons can either fully occupied the t_{2g} orbitals forming $S = 0$ LS state or the Hund's rule is prevailed forming $S = 2$ HS state. Recent studies showed that $[Fe^{II}(Pyrz)_2]$ deposited on inert metallic surface preserves the spin state switching.[21–23,26,27,34]

The Au/Co/Au(111) system, which has been studied in all detail due to its spin reorientation transition and spintronic applications,[39–45] was used as a ferromagnetic substrate with inert surface for molecular deposition. Due to the lower free surface energy of Au in comparison with Co, Au shows the tendency for up diffusion when Co/Au(111) system was annealed such that the Co film tends to be covered by a monolayer of Au, as deduced from an analysis of STM images.[41] Moreover, a helium atom scattering and Auger electron spectroscopy (AES) study revealed that this capping of the Co surface upon annealing is self terminated as evidenced by a saturation of the ratio of the highly surface sensitive AES lines of Co (53 eV)/Au (69 eV) at about 600 K.[46] Hand in hand with this saturation, the annealed surface shows an absence of CO adsorption upon titration at 180 K while CO sticks to Co even at room temperature indicating a full passivation.[46] More specifically, M. Speckmann et al.[39] reported that Co films of < 6 ML grown on Au(111) formed Au-terminated surface after an annealing process at 240° for 10–15 min producing a smooth and homogeneous Co film underneath. The magnetic properties of Co films are not quenched during annealing. Instead, the out-of-plane magnetic anisotropy is enhanced such that the spin reorientation of the magnetization from out-of-plane to in-plane shifts to higher thicknesses. For this study, we chose Co film thicknesses such that after Au up diffusion, the magnetization is still oriented in-plane although the passivation Au layer was on top. A more detailed description of the Co films growth is shown in Figure S1 (Supporting Information). Figure 1c,d shows representative STM topographic images of Co films on Au(111) surface before (1c) and after (1d) annealing. The morphology is similar to previous results[40,43] and shows that the Co film is dominated by random islands without thermal annealing but forms large flat terraces after annealing. The Au passivated surface shows a moiré pattern on the surface that is absent before annealing. The moiré structure is characteristic for the lattice misfit between Co and Au and has also been observed on thinner Co films on Au(111).[43,47,48] After annealing, the orientation of magnetization in the Co film was verified to be in-plane by in situ magneto-optical Kerr effect (MOKE) measurements, showing a low coercivity of ≈ 5 mT (see Figure S1b, Supporting Information). After these processes, the $[Fe^{II}(Pyrz)_2]$ molecules were deposited onto the substrate held at room temperature from a Knudsen cell at 175°.

Figure 2a shows the topography of a sub-ML $[Fe^{II}(Pyrz)_2]$ molecular film on Au-passivated Co/Au(111) surface. The molecules form self-assembled single-layer islands with an apparent height of 0.6 nm (Figure 2b), which is compatible with the height of the molecules grown directly on the Au(111) surface.[21] This is in contrast to molecules deposited directly on Co surfaces, where no ordered structures of the molecules form. The absence of disordered molecular adsorption pinpoints again a full passivation of the Co layer. Moreover, the molecules

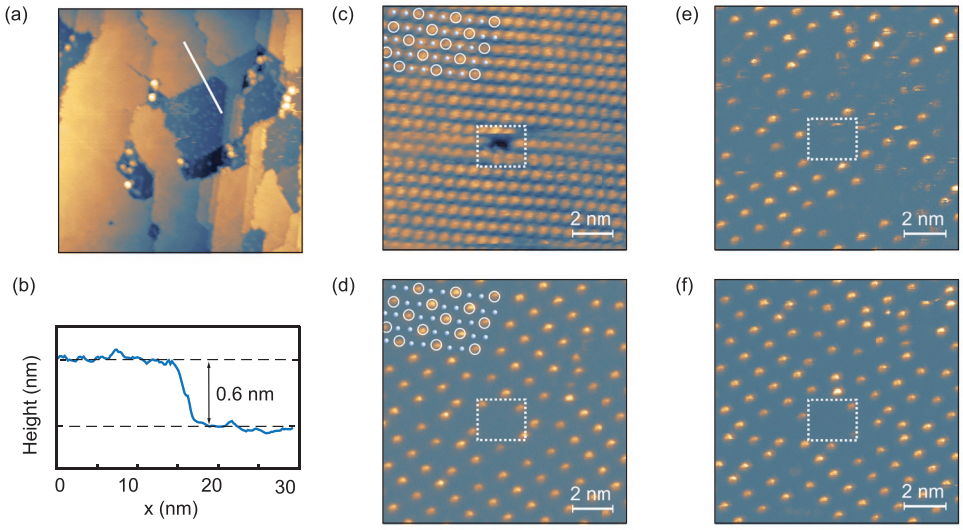

Figure 2. a) STM topography of self-assembled $[Fe^{II}(Pyrz)_2]$ molecules on Au-passivated Co/Au(111) (U = -1 V, I = 50 pA, 85 nm × 85 nm). b) The line profile across the border of the molecular island as marked with white solid line in (a). c,d) STM images acquired at same scanning area in constant-current mode (c) (U = -2 V, I = 50 pA) and constant-height mode (d) (U = 300 mV, $\langle I \rangle$ = 50 pA) showing patterns of different period. The former shows a full molecular crystal lattice, that is, both HS and LS molecules are visible, while the latter, under the specific voltage, only LS molecules appear as bright dots showing a mixed spin-state superstructure. The white circles (dots) mark the molecules in LS (HS) states and are the guide for the eyes. e) Constant-height images (U = 300 mV, $\langle I \rangle$ = 50 pA), acquired right after scanning the area at -2 V, showing a perturbed pattern. Some molecules fluctuate between HS and LS states. f) Constant-height image (U = 300 mV, $\langle I \rangle$ = 50 pA) acquired after 70 min after (e). The molecules relax to a more ordered pattern. Figure 2c–f is acquired at the same scanning area. The dashed rectangle is a mark of the defect for clarity. Image (d) was acquired after 3 h after (e).

deposited onto Au-passivated Co/Au(111) surface here, show an identical superstructure pattern as in the case of deposition on bare Au(111). Identically to previous studies on bare Au,[21] when imaged at -2 V (Figure 2c), all the molecules under the scanning area are visible showing a well-ordered 1×1 lattice pattern. However, for the same area, when scanned at 0.3 V with constant-height scanning mode, only a fraction of (1/3) the molecules is visible as partially indicated by the white circles in Figure 2d. The other 2/3 molecules on the sites marked by white dots are invisible. The appearing 1/3 bright molecules were initially identified as molecules in the HS state,[21] which were recently corrected as molecules in the LS state.[26] Thus, we conclude from the STM experiments, at 4 K, 1/3 of the molecules are in the LS state and 2/3 in the HS state showing LS-HS-HS pattern, that is, the spin-state structure of the molecules on the passivated Co film is identical to that observed on bare Au(111).

The molecules on Au-passivated Co/Au(111) surface are sensitive to the scanning bias and SCO can be triggered by scanning at certain applied voltage. Figure 2e,f shows this unique behavior. After scanning at high bias (-2 V), the LS-HS-HS ordered pattern is modified, some molecules are switched from LS (HS) state to HS (LS) state temporarily (Figure 2e) and reorganize into the LS-HS-HS pattern (Figure 2f) after about 1 h. Let the system relaxed for a longer time (about 3 h), the molecules form nearly defect-free pattern as shown in Figure 2d. The recovery of the ordered pattern give a first hint that SCO is present for the molecules adsorbed on the passivated FM substrate.

To directly look into the on-surface spin state switching of the molecules, we investigated thermal SCO of the hybrid system using soft X-ray absorption spectroscopy (XAS). XAS is a powerful technique for revealing the electronic structure of the 3d electrons of the Fe ions.[27] Different spin states, that is, HS or LS, have a rather clear fingerprint XAS on Fe $L_{2,3}$ adsorption edges. XAS has also been used to resolve the HS and LS contents quantitatively.[19,27] **Figure 3**a shows the XAS spectra of powder [$Fe^{II}(Pyrz)_2$] molecules at 300 K (100 K) representing the featured HS (LS)-state spectrum, as they show complete spin switching. Intuitively speaking, the molecules in HS states show a dominant adsorption peak at 707.7 eV, while that of the molecules in LS states is at 709.2 eV. Note that the powder spectra were taken at the DEIMOS beamline of SOLEIL synchrotron,[38] while the following data were taken at the WERA beamline of KARA,[49] so an energy shift has been applied to allow direct comparison of the spectra. To determine the HS/LS content on the hybrid system, the powder spectra were used as a reference. Figure 3b,c shows two exemplary XAS spectra of sub-ML [$Fe^{II}(Pyrz)_2$] molecules on Au-passivated Co/Au(111) surface measured at 300 and 60 K. The spectra show clear differences at both Fe L_2 and L_3 edges. The sub-ML film spectrum measured at 300 K shows an almost identical structure as the powder spectrum at high temperature indicating a high HS content. The spectrum measured at 60 K shows features at both peak positions of HS and LS, indicating coexistence of the two spin states. Quantitative analysis is shown in Figure 3d,e. Here we fitted the molecular film XAS spectra by a linear combination of the HS and LS powder spectra giving the contribution from HS and LS spectra, that is, the population of the spin states as a function of temperature.[19,27] More details can be found in Supporting Information. As shown in Figure 3d,e, the calculated spectra reproduce all main features of the experimental spectra, showing a calculated HS proportion of 93.9 % ± 0.8 % (72.7 % ± 1.4 %) for sub-ML molecules on Au/Co/Au(111) at 300 K (60 K).

To further elucidate the thermal switching, we record a series of XAS spectra from 300 to 30 K and extract the corresponding HS ratio as a function of temperature by the method mentioned above. The resulting HS proportion measured with XAS using an estimated photon flux density of the order of

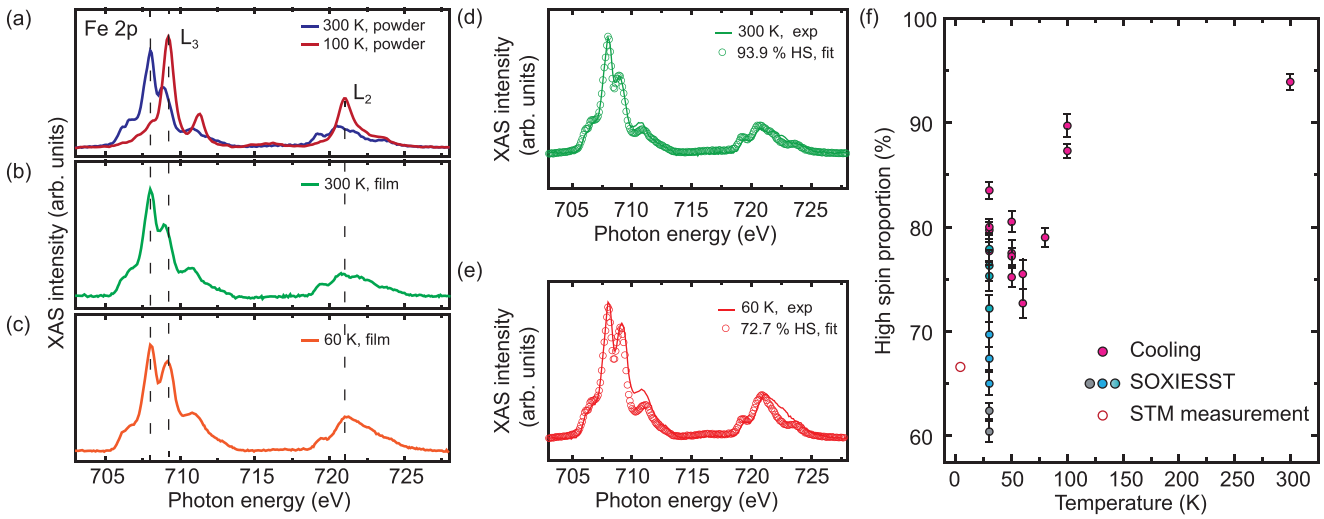

Figure 3. a) XAS spectra of powder [$Fe^{II}(Pyrz)_2$] molecules obtained at 300 K (blue) and 100 K (red) showing the HS-state (blue) and LS-state (red) featured spectra. b,c) XAS spectra of sub-monolayer [$Fe^{II}(Pyrz)_2$] film on Co/Au(111) obtained at 300 K (b) and 60 K (c). The dashed lines indicate the Fe L_2 and L_3 edges. d,e) Reproduction of Fe 2p XAS in Figure 2b,c by using a linear combination the reference spectra from Figure 2a for the HS and LS states obtained on the powder sample. The solid lines represent the experimental data and the circles represent the reproduced spectra obtained by linear combination. f) HS proportion of the molecules measured during cooling process (magenta circles) and the evolution of the HS population during SOXIESST effect under irradiation of different photon flux densities of X-rays (gray circles: low, blue circles: medium, and green circles: high flux densities). The open circle represents the data point measured by STM which shows 2/3 HS state molecules. Error bars indicate the 1σ statistical error of the spectral fit.

9×10^9 photons per (mm^2 s) during cooling process is shown in Figure 3f in magenta dots. This photon flux density is similar to that used in previous studies of the same molecules.[18,38] As can be seen from the figure, the molecules show thermal SCO slightly <100 K, that is, the HS population decreases, and soft X-ray induced excited spin states trapping (SOXIESST) at temperatures <60 K, that is, the HS population increases again driven by the X-ray photons. A more detailed analysis of SOXIESST will be discussed, below. We also included information on the HS population from the STM experiments at 4 K in Figure 3f confirming the identification of the appearing bright molecules as the LS species.

As evidenced by the data, the SOXIESST-induced LS to HS switching is not negligible at temperatures < 60 K. To gain further insight on the SOXIESST effect, we record the evolution of the XAS spectra under irradiation of soft X-ray at 30 K. To avoid the accumulation of the SOXIESST effect from the measurements during the cooling process, the measurement was taken at a virgin area and we exposed the sample to different flux densities of X-ray, marked as low/medium/high intensity (see Supporting Information for detailed definition). To maximize the resolution of the measurements with respect to the photon dose, we recorded the evolution of only the dominant adsorption peaks of Fe 2p L_3 edge, that is, shortening the exposure time per spectrum. **Figure 4**a shows a series of XAS spectra at the Fe L_3 edge measured under X-ray irradiation. To clearly elaborate the evolution process, we normalize the XAS spectra to t_{2g} peak, that is, the peak at 707.7 eV, and observe the changes of e_g peaks. Obviously, the e_g peak decreases relative to the t_{2g} peak with X-ray irradiation (red arrow), indicating an increase of HS state molecules. To analyze the data in detail, we fitted the spectra with a linear combination of the powder spectra to obtain the HS/LS ratio. The resulting HS proportion is shown in Figure 4b as a function of the irradiation time to the different X-ray flux densities. Under the irradiation of low flux density X-rays, the molecules show an almost constant HS proportion for at least 30 min, representing a negligible SOXIESST effect. After increasing the X-ray flux density, we observed a continuous SOXIESST-mediated LS to HS switching increasing the HS population by about 10 %. The switching dynamics can be well fitted with a mono-exponential function showing a time constant (τ) of 17.7 ± 5.5 min. Moreover, by applying a even higher X-ray flux density, more of the residual LS molecules can be switched to the HS state and eventually the HS molecules are saturated at around 76 %. For this process, the fitted τ is 3.1 ± 1.4 min. It is worthy to mention that the calculated activation energy, that is ($\tau \times I_0$), where I_0 is the flux density of applied X-ray, for both cases are nearly the same, which means that the microscopic origin of the switching process is independent of the X-ray flux density.

For comparison, we plot the data points of SOXIESST-mediated LS to HS switching together with the cooling data in Figure 3f. We note that the HS proportion achieved during cooling under X-ray is higher than during gradual exposure to X-rays at 30 K indicating that some portion of the molecules can only be kept in the HS state by X-rays when the temperature is higher than 30 K. The mechanism for this behavior is unclear. The original HS proportion (around 60 %) measured at 30 K is slightly deviated from the value (2/3) decided by STM can be due to the different measurement ranges, that is, STM focus on the interior of molecular islands and neglects edges effects while the beam size of XAS measurements here was around 0.5–1.5 mm^2. The edges and defects might contribute to pin down the LS states resulting in a slightly lower HS proportion.

The above experiments clearly indicate that the molecules deposited on passivated FM Co/Au(111) surface preserve bistability. The SCO can be triggered by the tunneling bias, be engineered thermally and by applying X-ray irradiation. The molecules on the passivated Co films show the very same behavior with incomplete spin-switching, as has been reported for molecules deposited on bare Au(111),[21] that is, the passivation fully works. With these results, we now turn to the possible magnetic interaction between the HS molecules and the FM Co film. For this purpose, synchrotron-based XMCD measurements were performed on Co and Fe *L*-edge with circularly polarized photons. **Figure 5**a shows the experimental geometry and setup.

The difference of the XAS spectra obtained with antiparallel relative orientation of photon spin and external field direction and parallel relative orientation is defined as the XMCD signal.[50,51] We ensured that the Co film was fully saturated

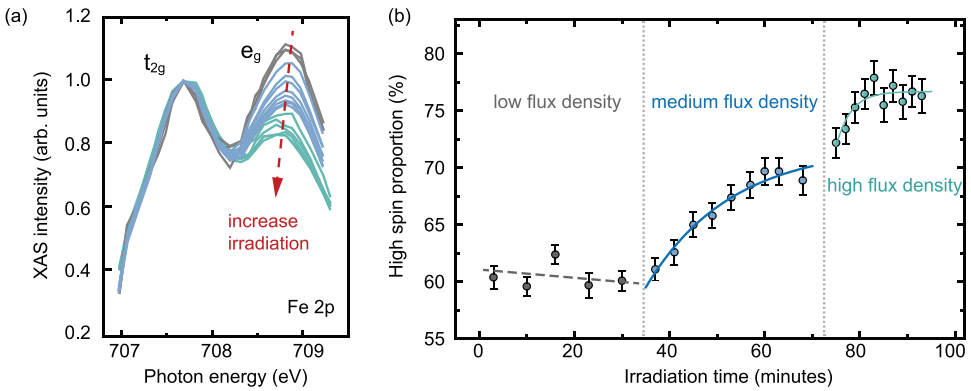

Figure 4. a) Evolution of XAS spectra obtained under irradiation with soft X-rays. The spectra were normalized to t_{2g} peak of Fe 2p L_3 edge for comparison. A clear change of the peak ratio (t_{2g}/e_g) as indicated by the red arrow corresponds to continuous increases of the HS population. b) Time evolution of the HS fraction under irradiation of soft X-ray at different photon flux densities. The gray/blue/green circles represent the data points obtained under exposure to the soft X-ray with low/medium/high photon flux densities. The corresponding blue (green) lines show an exponential fit of the data with a time constant of 17.7 ± 5.5 (3.1 ± 1.4) min. The dashed lines are the guides of the eyes. Error bars indicate the 1σ error of the spectral fit.

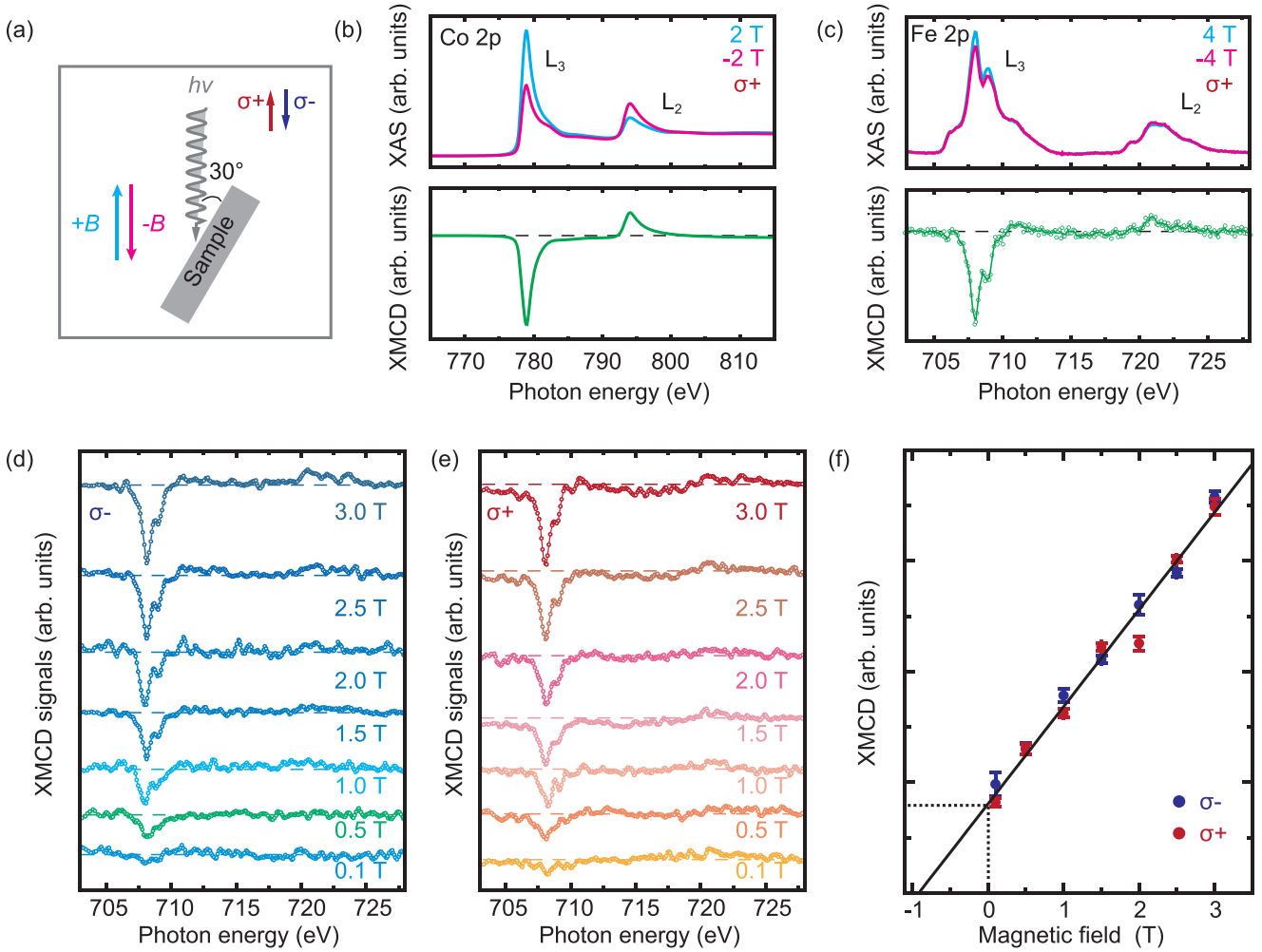

Figure 5. a) Schematic of experimental geometry with circularly polarized X-rays impinging the sample under grazing incidence with 30°. The σ^+ (σ^-) corresponds to positive (negative) photon helicity. b) Co *L*-edge XAS and XMCD spectra at 30 K measured with positive helicity photons (σ^+) and a magnetic field of 2 T. c) Fe *L*-edge XAS and XMCD spectra at 30 K taken in analogy to b) with 4 T. The green circles represent the experimental data and the green solid line is the smooth result of the points for the guide of eyes. d,e) Magnetic field dependent XMCD signal across the Fe $L_{2,3}$ edges measured with different photon helicity. (d): σ^-; (e): σ^+. The curves are vertically shifted for clarity and the dashed lines mark the zero signal positions. f) XMCD signals extracted from (d,e), that is the blue dots correspond to negative helicity (σ^-) measurements, and the red dots correspond to positive helicity (σ^+) measurements. The solid black line indicates the fit according to Brillouin function, showing a non-zero XMCD signal at extrapolated zero applied field. Error bars represent the 1σ statistical error of the XMCD signal.

by the applied magnetic filed by also measuring its hysteresis using the Co XMCD signal (see Figure S1c, Supporting Information). The amplitude and sign of the XMCD signal represent the size and orientation of the magnetic moment of the selected element. This enables us to probe the molecular magnetic properties and identify the type of coupling between the molecules and the substrate. Figure 5b,c shows the XAS spectra recorded with circularly polarized photons with position helicity (σ^+) across the Co and Fe *L*-edge respectively (upper panel) and the corresponding XMCD signal (lower panel). The same sign of the XMCD signal infers that the alignment of the Co and Fe magnetic moment is parallel, hinting at a ferromagnetic exchange coupling between the underlying Co film and HS molecules.[52] In principle, paramagnetic HS molecules can be aligned by the external magnetic field and contribute to the XMCD signal as well. Therefore, distinguishing and extracting the exchange-interaction contribution from the paramagnetic response is of paramount importance. To disentangle the two, we thus performed a series of XMCD measurements at different magnetic fields. As can be seen from Figure 5d,e, the XMCD signal gradually increases upon increasing the applied magnetic field, which is in line with the expectation of paramagnetic response. For quantitative analysis, we extract the XMCD signal and fit the data with the Brillouin function which describes the magnetization of paramagnet. We treat a potential exchange interaction from Co film to HS molecules as an effective exchange field B_{ex}, that acts together with the applied magnetic field $B_{applied}$. This scenario can result in the Brillouin function offset by the exchange field:

$$B_J(x) = \frac{2J+1}{2J}\coth\left(\frac{2J+1}{2J}x\right) - \frac{1}{2J}\coth\left(\frac{1}{2J}x\right), \quad (1)$$

where $x = J\frac{g\mu_B(B_{\text{applied}} + B_{\text{ex}})}{k_B T}$, g is the Landé factor, μ_B the Bohr magneton, T the temperature, k_B the Bolzmann constant, J the total angular momentum. For HS $[Fe^{II}(Pyrz)_2]$ molecule, $J = 2$. This equation, with the applied magnetic fields (≤ 3 T) and temperature (30 K), can be simplified as:

$$B_J(x) = C * (B_{\text{applied}} + B_{\text{ex}}) \quad (2)$$

with C a constant. More detail can be found in supplemental materials. The result of a fit to this model and the extracted XMCD signals are together presented in Figure 5f. A non-zero exchange interaction results in a non-zero XMCD signal at extrapolated zero applied field. The fit clearly does not extrapolate to zero magnetization at zero applied field and instead indicates a substantial ferromagnetic exchange field of $B_{\text{ex}} = 918 \pm 41$ mT. Compared to the SCO molecule $[Fe(phen)_2(NCS)_2]$ on Co/Cu(111),[20] the coupling is lower. This can be due to (i) the passivation of the Co film by the Au layer[39] that mediates an indirect exchange of the HS molecules[36] and Co films and (ii) the intrinsic decoupling of the molecules spin by the ligands that surround the Fe(II) ion. However, at the same time, both of the side effects help to preserve the spin switching ability when deposited on the FM functional substrate.

3. Conclusion

In conclusion, we demonstrated that the SCO properties of $[Fe^{II}(Pyrz)_2]$ molecules can be kept even on a magnetic substrate, if it is passivated by a noble metal overlayer. In the hybrid film, the HS to LS switching is thermally induced around 100 K while the reverse LS to HS transition is induced at 30 K by soft X-ray irradiation. Most interestingly, we have observed a sizable exchange coupling between the HS molecules and the FM substrate. This study allows to get insight into the influence of this functional SCO-FM substrate hybrid structure, both with respect to SCO and the exchange interaction between the HS molecules and the FM cobalt through the passivation layer making applications of hybrid systems come closer to reality. For FM films of low coercivity, thermal or light induced SCO might lead to changes of the magnetic behavior of the coupled hybrid system, that is, the SCO molecules might influence the magnetic behavior of the FM film mediated by the exchange interaction.

4. Experimental Section

*Sample Preparation:*The synthesis of $[Fe^{II}(Pyrz)_2]$ powder was shown in the previous works.[38] First, a clean Au(111) substrate was prepared by repeated cycles of Ar^+ sputtering (3 kV) and post-annealing (450 °C) in ultrahigh vacuum (UHV). Subsequently, Co films were deposited onto the clean Au(111) surface held at room temperature by e-beam evaporator. The thickness of the Co film was determined by deposition rate and deposition time (see Section 1, Supporting Information). Here, the thickness of Co film is determined to be 7.2 ± 0.9 monolayers (MLs). To form a flat and passivated surface, the Co/Au(111) film was then post-annealed at 300 °C for 30 min. We in situ monitored the magnetic properties of the Co films before and after annealing by magneto-optical Kerr effect (MOKE) measurement. They showed an in-plane magnetization of the Co films (see Figure S1b, Supporting Information). After that, the molecules were deposited onto the as mentioned passivated Co/Au(111) substrate in UHV using a homemade Knudsen cell evaporator at 175 °C while keeping the substrate at room temperature. The thickness of the molecules is determined to be 0.75 ± 0.08 ML by STM.

*STM Experiments:*The measurements were performed in a home-built STM operating at a base temperature of 4.5 K and base pressure under 1×10^{-10} mbar.

*X-Ray Absorption Spectroscopy and X-Ray Magnetic Circular Dichroism Measurements:*XAS and XMCD measurements were performed at IQMT's soft x-ray facility WERA at the Karlsruhe synchrotron light source KARA, utilizing the XMCD end station with its fast-ramp 7 T magnet. Total electron yield (TEY) detection was used. Base pressure at WERA is better than 1×10^{-10} mbar. To prevent any sample contamination in air, the freshly prepared samples, after in situ characterization with STM, were transferred directly to the XMCD loadlock at WERA via a customized UHV suitcase with a base pressure better than 1×10^{-9} mbar.

Supporting Information

Supporting Information is available from the Wiley Online Library or from the author.

Acknowledgements

The authors acknowledge funding by the DFG under grant Wu 349/13-1. The authors thank Vincent Davense for providing the original XAS data files from powder samples and Michael Merz for fruitful discussions. A.B.G. and J.A.R. thank the Spanish Ministerio de Ciencia e Innovación (grant PID2019-106147GB-I00 funded by MCIN/AEI/10.13039/501100011033) and Unidad María de Excelencia María de Maeztu (CEX2019-000919-M). The authors were grateful to the Karlsruhe synchrotron light source KARA for the provision of beamtime. The authors thank E. Goering (MPI-IS Stuttgart, Germany) for the use of their XMCD endstation.

Open access funding enabled and organized by Projekt DEAL.

Conflict of Interest

The authors declare no conflict of interest.

Data Availability Statement

The data that support the findings of this study are available from the corresponding author upon reasonable request.

Keywords

exchange interaction, ferromagnetic coupling, molecular magnetism, spin-crossover molecules

Received: February 2, 2023
Published online:

[1] P. Gütlich, A. Hauser, H. Spiering, *Angew. Chem. Int. Ed.* **1994**, *33*, 2024.
[2] P. Gütlich, H. A. Goodwin, editors, *Spin Crossover in Transition Metal Compounds I-III*, Springer Berlin, Heidelberg **2004**.

[3] J. A. Real, A. B. Gaspar, M. C. Muñoz, *Dalton Trans.* **2005**, 2062.
[4] M. A. Halcrow, editor, *Spin-crossover materials: Properties and applications*, John Wiley and Sons Ltd, Hoboken **2013**.
[5] A. Bousseksou, Editor, C. R. Chim **2018**, *21*, 1055.
[6] A. B. Gaspar, G. Molnár, A. Rotaru, H. J. Shepherd, *C. R .Chim* **2018**, *21*, 1095.
[7] L. Kipgen, M. Bernien, F. Tuczek, W. Kuch, *Adv. Mater.* **2021**, *33*, 2008141.
[8] M. Gruber, V. Davesne, M. Bowen, S. Boukari, E. Beaurepaire, W. Wulfhekel, T. Miyamachi, *Phys. Rev. B* **2014**, *89*, 195415.
[9] G. Molnár, S. Rat, L. Salmon, W. Nicolazzi, A. Bousseksou, *Adv. Mater.* **2018**, *30*, 17003862.
[10] K. S. Kumar, M. Ruben, *Angew Chem. Int. Ed.* **2021**, *60*, 7502.
[11] K. S. Kumar, M. Ruben, *Coord. Chem. Rev.* **2017**, *346*, 176.
[12] K. S. Kumar, M. Studniarek, B. Heinrich, J. Arabski, G. Schmerber, M. Bowen, S. Boukari, E. Beaurepaire, J. Dreiser, M. Ruben, *Adv. Mater.* **2018**, *30*, 1705416.
[13] A. Bellec, J. Lagoute, V. Repain, *C.R.Chim* **2018**, *21*, 1287.
[14] M. Gruber, R. Berndt, *Magnetochemistry* **2020**, *6*, 3.
[15] A. C. Aragonès, D. Aravena, J. I. Cerdá, Z. Acís-Castillo, H. Li, J. A. Real, F. Sanz, J. Hihath, E. Ruiz, I. Díez-Pérez, *Nano Lett.* **2016**, *16*, 218.
[16] A. C. Aragonès, D. Aravena, F. J. Valverde-Muñoz, J. A. Real, F. Sanz, I. Díez-Pérez, E. Ruiz, *J. Am. Chem. Soc.* **2017**, *139*, 5768.
[17] L. Poggini, G. Londi, M. Milek, A. Naim, V. Lanzilotto, B. Cortigiani, F. Bondino, E. Magnano, E. Otero, P. Sainctavit, M.-A. Arrio, A. Juhin, M. Marchivie, M. M. Khusniyarov, F. Totti, P. Rosa, M. Mannini, *Nanoscale* **2019**, *11*, 20006.
[18] V. Davesne, M. Gruber, M. Studniarek, W. H. Doh, S. Zafeiratos, L. Joly, F. Sirotti, M. G. Silly, A. B. Gaspar, J. A. Real, G. Schmerber, M. Bowen, W. Weber, S. Boukari, V. Da Costa, J. Arabski, W. Wulfhekel, E. Beaurepaire, *J. Chem. Phys.* **2015**, *142*, 194702.
[19] T. Miyamachi, M. Gruber, V. Davesne, M. Bowen, S. Boukari, L. Joly, F. Scheurer, G. Rogez, T. K. Yamada, P. Ohresser, E. Beaurepaire, W. Wulfhekel, *Nat. Commun.* **2012**, *3*, 938.
[20] S. Gueddida, M. Gruber, T. Miyamachi, E. Beaurepaire, W. Wulfhekel, M. Alouani, *J. Phys. Chem. Lett.* **2016**, *7*, 900.
[21] K. Bairagi, O. Iasco, A. Bellec, A. Kartsev, D. Li, J. Lagoute, C. Chacon, Y. Girard, S. Rousset, F. Miserque, Y. J. Dappe, A. Smogunov, C. Barreteau, M. L. Boillot, T. Mallah, V. Repain, *Nat. Commun.* **2016**, *7*, 12212.
[22] M. Kelai, V. Repain, A. Tauzin, W. Li, Y. Girard, J. Lagoute, S. Rousset, E. Otero, P. Sainctavit, M.-A. Arrio, M.-L. Boillot, T. Mallah, C. Enachescu, A. Bellec, *J. Phys. Chem. Lett.* **2021**, *12*, 6152.
[23] Y. Tong, M. Kelaï, K. Bairagi, V. Repain, J. Lagoute, Y. Girard, S. Rousset, M.-L. Boillot, T. Mallah, C. Enachescu, A. Bellec, *J. Phys. Chem. Lett.* **2021**, *12*, 11029.
[24] C. Fourmental, S. Mondal, R. Banerjee, A. Bellec, Y. Garreau, A. Coati, C. Chacon, Y. Girard, J. Lagoute, S. Rousset, M.-L. Boillot, T. Mallah, C. Enachescu, C. Barreteau, Y. J. Dappe, A. Smogunov, S. Narasimhan, V. Repain, *J. Phys. Chem. Lett.* **2019**, *10*, 4103.
[25] N. Konstantinov, A. Tauzin, U. N. Noumbé, D. Dragoe, B. Kundys, H. Majjad, A. Brosseau, M. Lenertz, A. Singh, S. Berciaud, M.-L. Boillot, B. Doudin, T. Mallah, J.-F. Dayen, *J. Mater. Chem. C* **2021**, *9*, 2712.
[26] L. Zhang, Y. Tong, M. Kelai, A. Bellec, J. Lagoute, C. Chacon, Y. Girard, S. Rousset, M.-L. Boillot, E. Rivière, T. Mallah, E. Otero, M.-A. Arrio, P. Sainctavit, V. Repain, *Angew. Chem. Int. Ed.* **2020**, *59*, 13341.
[27] K. Bairagi, A. Bellec, C. Fourmental, O. Iasco, J. Lagoute, C. Chacon, Y. Girard, S. Rousset, F. Choueikani, E. Otero, P. Ohresser, P. Sainctavit, M.-L. Boillot, T. Mallah, V. Repain, *J. Phys. Chem. C* **2018**, *122*, 727.
[28] G. Hao, A. Mosey, X. Jiang, A. J. Yost, K. R. Sapkota, G. T. Wang, X. Zhang, J. Zhang, A. T. N'Diaye, R. Cheng, X. Xu, P. A. Dowben, *Appl. Phys. Lett.* **2019**, *114*, 032901.
[29] S. Thakur, E. Golias, I. Kumberg, K. Senthil Kumar, R. Hosseinifar, J. Torres-Rodríguez, L. Kipgen, C. Lotze, L. M. Arruda, C. Luo, F. Radu, M. Ruben, W. Kuch, *J. Phys. Chem. C* **2021**, *125*, 13925.
[30] F. Prins, M. Monrabal-Capilla, E. A. Osorio, E. Coronado, H. S. J. van der Zant, *Adv. Mater.* **2011**, *23*, 1545.
[31] H. J. Shepherd, I. A. Gural'skiy, C. M. Quintero, S. Tricard, L. Salmon, G. Molnár, A. Bousseksou, *Nat. Commun.* **2013**, *4*, 2607.
[32] C. Boix-Constant, V. García-López, E. Navarro-Moratalla, M. Clemente-León, J. L. Zafra, J. Casado, F. Guinea, S. Mañas-Valero, E. Coronado, *Adv. Mater.* **2022**, *34*, 2110027.
[33] R. Torres-Cavanillas, M. Morant-Giner, G. Escorcia-Ariza, J. Dugay, J. Canet-Ferrer, S. Tatay, S. Cardona-Serra, M. Giménez-Marqués, M. Galbiati, A. Forment-Aliaga, E. Coronado, *Nat. Chem.* **2021**, *13*, 1101.
[34] M. Gavara-Edo, R. Córdoba, F. J. Valverde-Muñoz, J. Herrero-Martín, J. A. Real, E. Coronado, *Adv. Mater.* **2022**, *34*, 2202551.
[35] M. Bernien, H. Naggert, L. M. Arruda, L. Kipgen, F. Nickel, J. Miguel, C. F. Hermanns, A. Krüger, D. Krüger, E. Schierle, E. Weschke, F. Tuczek, W. Kuch, *ACS Nano* **2015**, *9*, 8960.
[36] M. Gruber, F. Ibrahim, S. Boukari, L. Joly, V. Da Costa, M. Studniarek, M. Peter, H. Isshiki, H. Jabbar, V. Davesne, J. Arabski, E. Otero, F. Choueikani, K. Chen, P. Ohresser, W. Wulfhekel, F. Scheurer, E. Beaurepaire, M. Alouani, W. Weber, M. Bowen, *Nano Lett* **2015**, *15*, 7921.
[37] O. Iasco, M.-L. Boillot, A. Bellec, R. Guillot, E. Rivière, S. Mazerat, S. Nowak, D. Morineau, A. Brosseau, F. Miserque, V. Repain, T. Mallah, *J. Mater. Chem. C* **2017**, *5*, 11067.
[38] V. Davesne, M. Gruber, T. Miyamachi, V. Da Costa, S. Boukari, F. Scheurer, L. Joly, P. Ohresser, E. Otero, F. Choueikani, A. B. Gaspar, J. A. Real, W. Wulfhekel, M. Bowen, E. Beaurepaire, *J. Chem. Phys.* **2013**, *139*, 074708.
[39] M. Speckmann, H. P. Oepen, H. Ibach, *Phys. Rev. Lett.* **1995**, *75*, 2035.
[40] B. Voigtländer, G. Meyer, N. M. Amer, *Phys. Rev. B* **1991**, *44*, 10354.
[41] S. Padovani, F. Scheurer, J. P. Bucher, *Europhys. Lett.* **1999**, *45*, 327.
[42] R. Allenspach, M. Stampanoni, A. Bischof, *Phys. Rev. Lett.* **1990**, *65*, 3344.
[43] N. Haag, M. Laux, J. Stöckl, J. Kollamana, J. Seidel, N. Großmann, R. Fetzer, L. L. Kelly, Z. Wei, B. Stadtmüller, M. Cinchetti, M. Aeschlimann, *New J. Phys.* **2016**, *18*, 103054.
[44] B. Miao, Y. Millev, L. Sun, B. You, W. Zhang, H. Ding, *Sci. China: Phys., Mech.* **2013**, *56*, 70.
[45] S. Pütter, H. F. Ding, Y. T. Millev, H. P. Oepen, J. Kirschner, *Phys. Rev. B* **2001**, *64*, 092409.
[46] C. Tölkes, P. Zeppenfeld, M. Krzyzowski, R. David, G. Comsa, *Suf. Sci.* **1997**, *349*, 170.
[47] N. Marsot, R. Belkhou, H. Magnan, P. Le Fèvre, C. Guillot, D. Chandesris, *Phys. Rev. B* **1999**, *59*, 3135.
[48] K. Morgenstern, J. Kibsgaard, J. V. Lauritsen, E. Lægsgaard, F. Besenbacher, *Surf. Sci.* **2007**, *601*, 1967.
[49] P. Grüninger, M. Polek, M. Ivanović, D. Balle, R. Karstens, P. Nagel, M. Merz, S. Schuppler, R. Ovsyannikov, H. F. Bettinger, H. Peisert, T. Chassé, *J. Phys. Chem. C* **2018**, *122*, 19491.
[50] J.Stöhr,*J. Electron Spectrosc. Relat. Phenom.* **1995**, *75*, 253.
[51] G. van der Laan, A. I. Figueroa, *Coord. Chem. Rev.* **2014**, *277-278*, 95.
[52] M. Gruber, F. Ibrahim, S. Boukari, H. Isshiki, L. Joly, M. Peter, M. Studniarek, V. Da Costa, H. Jabbar, V. Davesne, U. Halisdemir, J. Chen, J. Arabski, E. Otero, F. Choueikani, K. Chen, P. Ohresser, W. Wulfhekel, F. Scheurer, W. Weber, M. Alouani, E. Beaurepaire, M. Bowen, *Nat. Mater.* **2015**, *14*, 981.